

Article

Response of Travertine Dam to Precipitation over the Past 800 Years in Zabuye Salt Lake, Southwestern Tibetan Plateau

Mingming Li ¹, Mianping Zheng ^{2,*}, Chuanyong Ye ^{2,*}, Chenguang Wang ³, Xuefei Zhang ², Xuefeng Wang ⁴ , Yuanyi Zhao ² and Yanbo Zhang ⁵

¹ College of Geoscience and Surveying Engineering, China University of Mining and Technology (Beijing), Beijing 100083, China; testlmm@126.com

² MNR Key Laboratory of Saline Lake Resources and Environments, Institute of Mineral Resources, Chinese Academy of Geological Sciences, Beijing 100037, China; zhangxuefei2000@163.com (X.Z.); yyizhao@126.com (Y.Z.)

³ Hebei Key Laboratory of Strategic Critical Mineral Resources, Hebei GEO University, Shijiazhuang 050031, China; chenguangwangcags@163.com

⁴ Key Laboratory of Cenozoic Geology and Environment, Institute of Geology and Geophysics, Chinese Academy of Sciences, Beijing 100029, China; xfwang@mail.iggcas.ac.cn

⁵ Training Base, Army Engineering University, Xuzhou 221004, China; dtzybo@163.com

* Correspondence: zhengmp2010@126.com (M.Z.); yechuanrong@cags.ac.cn (C.Y.)

Abstract: The Tibetan Plateau is known as the core area of the third pole of the Earth and is a key area for global climate change research. This study uses the Zabuye Salt Lake travertine dam as the research object and U–Th dating as the chronological framework and proposes that the carbon and oxygen isotopes of travertine can be used as a precipitation index through the analysis of hydrogen and oxygen isotopes of spring water, and petrology, mineralogy, carbon and oxygen isotopes of travertine. The precipitation records of Zabuye Salt Lake over the last 800 years show a dry condition in 1191–1374 AD (Medieval Warm Period), a humid condition in 1374–1884 AD (Little Ice Age), and a dry condition in 1884–1982 AD (Current Warm Period), indicating a warm–dry/cold–moist climate pattern, which is consistent with precipitation records from many places on the Tibetan Plateau. We preliminarily point out that travertine can record the evolution of paleoprecipitation (paleomonsoon) at least on the decadal–centennial scale. The Indian summer monsoon has been the main factor influencing precipitation change in Zabuye Salt Lake over the past 800 years, and the change in evapotranspiration intensity caused by temperature change driven by solar radiation is also an important factor affecting dry–moist change.

Keywords: travertine; paleoprecipitation; Zabuye Salt Lake; Tibetan Plateau



Citation: Li, M.; Zheng, M.; Ye, C.; Wang, C.; Zhang, X.; Wang, X.; Zhao, Y.; Zhang, Y. Response of Travertine Dam to Precipitation over the Past 800 Years in Zabuye Salt Lake, Southwestern Tibetan Plateau. *Minerals* **2022**, *12*, 916. <https://doi.org/10.3390/min12070916>

Academic Editors: Francesca Giustini and Mauro Brilli

Received: 26 June 2022

Accepted: 19 July 2022

Published: 21 July 2022

Publisher's Note: MDPI stays neutral with regard to jurisdictional claims in published maps and institutional affiliations.



Copyright: © 2022 by the authors. Licensee MDPI, Basel, Switzerland. This article is an open access article distributed under the terms and conditions of the Creative Commons Attribution (CC BY) license (<https://creativecommons.org/licenses/by/4.0/>).

1. Introduction

The Tibetan Plateau is known as the core region of the Earth's third pole [1]. It is critical to the hemispheric and even the global atmospheric circulation system due to its huge area, geographic location, and high altitude [2], and is a key region of global climate change research [3]. The past 2000 years have been a key period for global climate change research, and a condition in 2000 years ago can be considered as a baseline for current conditions, as the climate has been very similar to the present [4]. The precipitation records of the Tibetan Plateau over the past 2000 years mainly come from tree rings [5–8], ice cores [9,10], and lake sediments [11–14]. Trees are mainly distributed in the eastern, northeastern, and southeastern parts of the plateau where the climate is suitable, and ice is mainly distributed at high altitudes where snowfall can be continuously preserved. Chronological control for nearly all published paleolimnological records from the Tibetan Plateau has been based on radiocarbon dating [15]; however, the radiocarbon age of lake sediments may be subject to reservoir effects due to the input of dead carbon from local bedrock or

wetlands within the catchment [16]. The reservoir effect has made it challenging to establish reliable chronologies for lake sediment cores from the Tibetan Plateau [15]. Little attention has been paid to high-resolution travertine sequences from the past 2000 years; however, travertine is a relatively common sedimentary phenomenon on the Tibetan Plateau and has great potential for environmental archives [17].

Travertine is a non-marine calcium carbonate deposited around springs, rivers, lakes, or caves, mainly composed of calcite and aragonite, and widely distributed in terrestrial environments [18–21]. Pentecost et al. divided it into meteogene and thermogene travertine according to the source of CO₂ in the environmental water. The former is also called tufa, and its carbon originates from soil CO₂ and carbonate rock, with δ¹³C mostly ranging from −12‰ to −2‰. The carbon of the latter comes from various sources, including hydrolysis and oxidation of reduced carbon and decarbonation of limestone or directly from the upper mantle, with δ¹³C usually ranging from −2‰ to 10‰ [20,22]. In Ford and Pedley's classification, tufa corresponds to meteogene travertine and travertine to thermogene travertine [19], and in this paper we use this term for discussion. For a long time, tufa was mainly used for paleoclimate reconstruction [23], and its resolution can reach years, seasons, months, and maybe even weeks [24–26]. Recently, more researchers have emphasized the close relationship between travertine distribution and climate [17,27–30]. Ricketts et al. compiled a global dataset containing 1649 published ages of travertine, which showed that although the deposition of travertine was spatially controlled by crustal faults and fractures, it was temporally regulated by global or regional climate change [31].

In the hinterland of the Tibetan Plateau, previous climate-related research was carried out on ancient travertine, which had ceased to grow and lacked the direct connection between modern spring (lake) water and its deposition [17,32–36]. Wang et al., based on a systematic study and a summary of their research results, proposed that the widely distributed travertine on the Tibetan Plateau could provide a record of paleoclimate (paleomonsoon) evolution at least over the decadal–centennial time scale [37]. Travertine dams are common in caves, springs, and rivers all over the world, ranging in size from millimeters to several meters [38,39].

This paper studied travertine based on U–Th dating, petrology, mineralogy, and carbon and oxygen isotopes as well as hydrogen and oxygen isotopes of spring (lake) water, taking the growing Zabuye Salt Lake travertine dam as the research object. We discussed the significance of travertine to the paleoenvironment in order to provide a basis for better use of travertine in reconstructing the climate of the Tibetan Plateau.

2. Geological Setting

Zabuye Salt Lake (31°14'47" N–31°33'10" N, 83°52'34" E–84°23'47" E) is located in the southwest of the Tibetan Plateau, at the intersection of the westerlies and the Indian summer monsoon (Figure 1), and is very sensitive to climate change. According to the meteorological data of the Long-Term Observation Station from 1991 to 2020, the annual average temperature in the Zabuye Salt Lake area is 3.1 °C, the annual average precipitation is 168.7 mm, and the annual average evaporation is 2579.1 mm. Precipitation is concentrated in the rainy season from early July to mid-September, which accounts for more than 90% of the total annual precipitation [40], indicating that summer monsoon rainfall dominates annual precipitation in the Zabuye Salt Lake area.

The Carboniferous and Permian strata are mainly distributed in the northern part of the Zabuye Salt Lake area, which consist of clastic and carbonate rocks. The Cretaceous is exposed in the south and southwest and the Paleogene in the east, and both are composed of clastic and volcanic rocks. The Neogene is distributed in the west and is a set of pyroclastic rocks. The Quaternary is mainly distributed around the lake, including residual slope, fluvial, lacustrine, and travertine deposits. The intrusive rocks in the salt lake area are mainly intermediate-acid rocks, ranging from diorite to granite (Figure 1c). The main structures are NW, NE, and nearly NS trending faults [42].

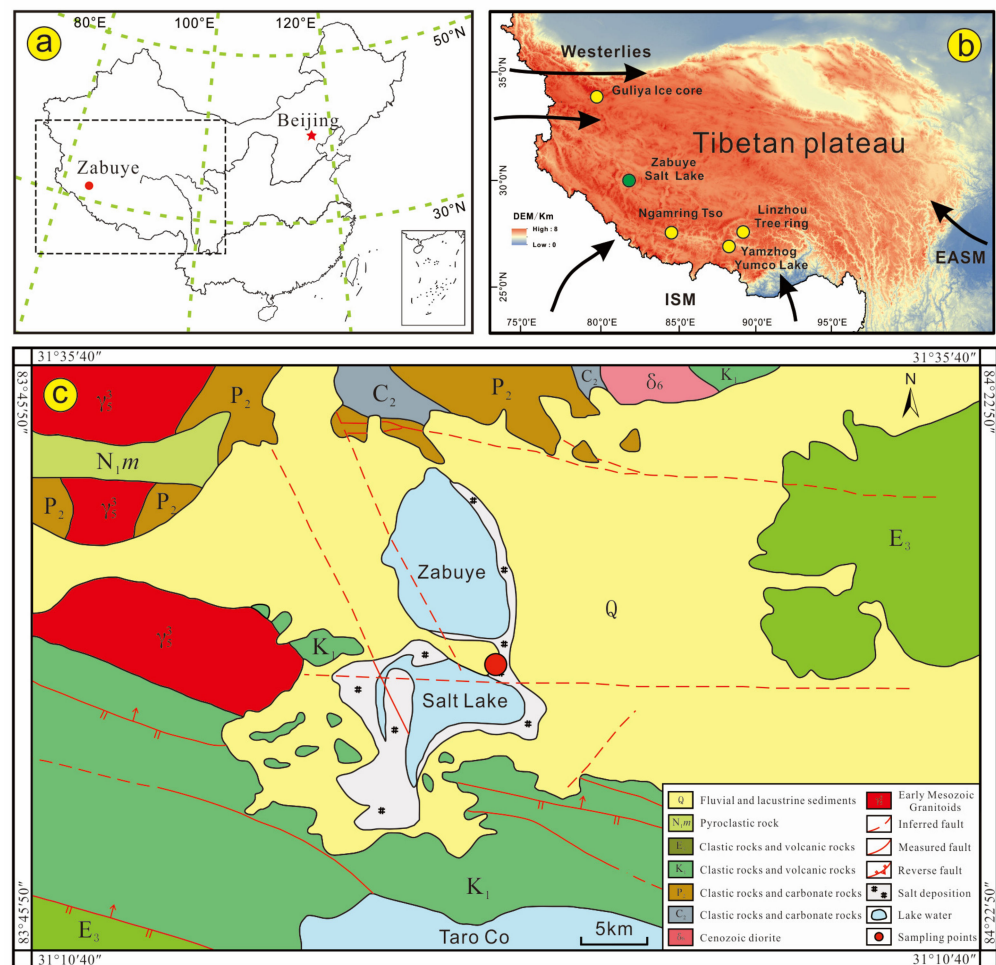


Figure 1. Maps of study site, Zabuye Salt Lake. (a,b) Zabuye Salt Lake and some related research sites on Tibetan Plateau: Guliya ice core [41], Ngamring Tso [13], Yamzhog Yumco Lake [11], and Linzhou tree rings [7]. EASM stand for the “East Asian summer monsoon”, ISM stand for the “Indian summer monsoon”, and DEM stand for the “Digital Elevation Model”. Black arrows indicate climate systems. (c) Simplified geological map of lake area.

Zabuye Salt Lake covers an area of 243 km² at an average elevation of about 4421 m. It is a semi-dry salt lake with a combination of surface brine and salt flats. Large-scale ancient travertine accumulation developed in the middle of the lake and formed a travertine island (Figure 1c). From the travertine island as the starting point to the west, a sand embankment was formed that divides Zabuye Lake into south and north lakes, and there is a waterway connecting the two on the east side. The springs around and in the lake are relatively well developed, and those on the travertine island have the largest water inflow [43].

3. Materials and Methods

3.1. Research Materials

There are many springs on Zabuye travertine island. The spring water flows into the salt lake and forms a travertine dam at the junction of the lake water. In this study, samples of spring water, lake water, and travertine were collected from a travertine dam with good topographic conditions (Figure 2). A 23.5 cm section was carved from the travertine dam, and a horizontal travertine bedding was developed (Figure 2e). A total of 24 samples (ZD01-24) were taken from top to bottom. Lake water samples (ZH01) and spring water samples (ZQ01) were taken from both sides of the travertine dam (Figure 2d), and one water sample (ZQ02) was taken from the spring hole. Travertine samples were transported back to the lab and dried in a drying oven at 50 °C.

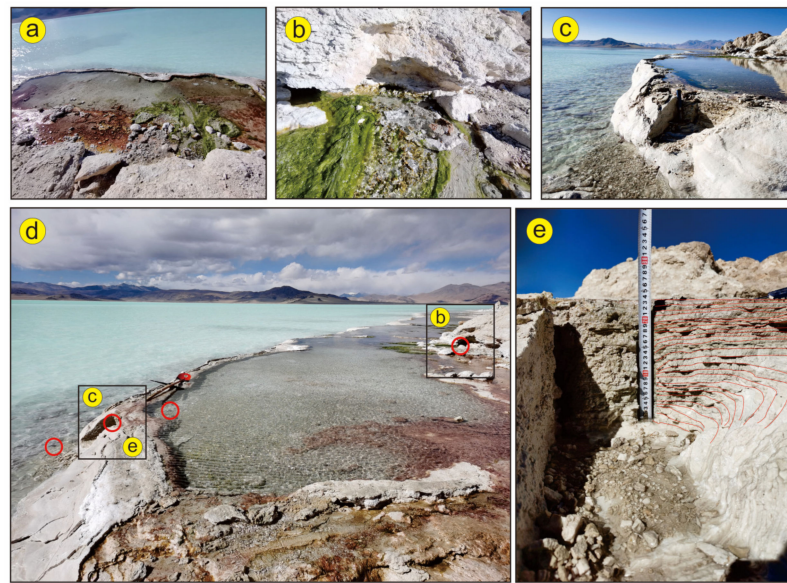


Figure 2. Outcrops of Zabuye Salt Lake. (a) Travertine dam formed by spring. (b) Spring outlet. (c–e) Close-up of travertine sampling sites, indicated by red circles. Black squares indicate the positions of (b,c,e).

3.2. Analytical Methods

3.2.1. U–Th Dating

Four travertine samples were collected for U–Th dating. Pure and compact calcite was selected as a test sample, and the impurities were washed with alcohol and hydrogen peroxide in an ultrasonic cleaning machine. The procedures for chemical separation and purification of uranium and thorium were similar to those in previous studies [44,45]. The $^{230}\text{Th}/^{232}\text{Th}$ atomic ratio of Zabuye Salt Lake water as the initial $^{230}\text{Th}/^{232}\text{Th}$ atomic ratio of $(6.7 \pm 0.67 \times 10^6)$ was used to correct the initial ^{230}Th amount. These samples were analyzed on a Thermo Fisher Neptune Plus multi-collector inductively coupled plasma mass spectrometer (MC-ICP-MS) at the Institute of Geology and Geophysics, Chinese Academy of Sciences, Beijing, China.

3.2.2. Petrography and Mineralogy

Petrographic and mineralogic observations of the travertine were conducted using a Leica DM4500P polarizing microscope on polished thin sections, and an FEI Nova NanoSEM 450 scanning electron microscope (with working condition of 20 kV and beam current of 15 μA) on carbon-coated samples. Thin sections were prepared and photographed at the MNR Key Laboratory of Saline Lake Resources and Environments, Beijing, China. The mineralogical composition analysis of travertine was performed by using a Bruker D2-PHASER X-ray diffractometer (Cu $K\alpha$, 30 kV, 10 mA, 7° – 90° 2θ , 0.02° 2θ step size, $6^\circ/\text{min}$) at the Sichuan University of Science and Engineering, Zigong, China. Quantified mineral results were analyzed with MDI Jade 6.5 software (Materials Data, Inc., Livermore, CA, USA). The MgCO_3 content of the carbonate minerals was calculated from the shift of d-spacing of the (104) reflection peak of calcite from their stoichiometric peak positions in the diffraction spectra [46,47]. Calcite with $<5\%$ MgCO_3 is classified as low-magnesium calcite (LMC), and calcite with $>5\%$ MgCO_3 is considered high-magnesium calcite (HMC). These are often denoted simply as calcite and magnesium calcite [48].

3.2.3. Stable Isotopes

Travertine carbon and oxygen isotopes were analyzed by using a Finnigan MAT 253 mass spectrometer. Carbon and oxygen isotopes were analyzed by the 100% phosphoric acid method, and analytical precision was $\pm 0.1\text{‰}$ for $\delta^{13}\text{C}$ and $\pm 0.2\text{‰}$ for $\delta^{18}\text{O}$. The

measurement results of carbon and oxygen isotopes were scaled by the V-PDB standard. Spring (lake) hydrogen and oxygen isotopes was measured by isotope ratio mass spectrometry. For the measurement of the $^{18}\text{O}/^{16}\text{O}$ ratio, the CO_2 equilibration method was employed; for the D/H ratio, H_2 was generated by the Zn-reduction method. Isotope ratios of CO_2 and H_2 were measured using a MAT-253 mass spectrometer, and the results are reported relative to V-SMOW with a standard deviation of $\pm 0.5\%$ and $\pm 0.1\%$. This work was done at the Analytical Laboratory of the Beijing Research Institute of Uranium Geology, Beijing, China.

4. Results

4.1. Chronology

The U–Th dating results are shown in Table 1 and Figure 3. The $^{230}\text{Th}/^{232}\text{Th}$ activity ratio of all samples is lower than 20, indicating that they are contaminated by ^{230}Th debris, so the age error has great uncertainty [49], and debris correction must be carried out [50]. The $^{230}\text{Th}/^{232}\text{Th}$ in Zabuye Lake water can represent the average value of detrital $^{230}\text{Th}/^{232}\text{Th}$ of the terrigenous detrital material transported into the lake from the periphery of the catchment basin. In this study, $^{230}\text{Th}/^{232}\text{Th}$ in Zabuye Salt Lake ($6.7 \pm 0.67 \times 10^6$) is used as the initial value of travertine for correction. ZD02 did not get effective age correction. Although the errors of ZD10, ZD17, and ZD24 age values are large, they have a good age sequence of lower old and higher new. By fitting the ages of ZD10, ZD17, and ZD24 samples to make the time-depth trend line of the travertine profile (Figure 3), the following formula can be obtained: $\text{Age} = 3.6305 \times D + 2.678$ ($R^2 = 0.9766$), where D is depth (mm) and R^2 is the square of the correlation coefficient. In this study, samples were collected in the field in 2020, and the top (0 mm) of the travertine profile was deposited, with a theoretical age of 0 years (-20 yr BP). According to the trend formula, the age of the top (0 mm) of the travertine profile was calculated to be 2.678 yr BP, with a difference of only about 23 yr. This indicates that U–Th dating can represent the age of travertine to a certain extent.

Table 1. ^{230}Th dating results for profiles in study area ($\pm 2\sigma$).

Sample	^{238}U	^{232}Th	$^{230}\text{Th}/^{232}\text{Th}$	$d^{234}\text{U}$	$^{230}\text{Th}/^{238}\text{U}$	^{230}Th Age (yr)	^{230}Th Age (yr)	$d^{234}\text{U}_{\text{Initial}}$	^{230}Th Age (yr BP)
	(ppb)	(ppt)	(Atomic $\times 10^{-6}$)	(Measured)	(Activity)	(Uncorrected)	(Corrected)	(Corrected)	(Corrected)
ZD10	4518 \pm 16	379,893 \pm 7712	7.6 \pm 0.2	748.8 \pm 4.1	0.0389 \pm 0.0003	2452 \pm 17	304 \pm 308	749 \pm 4	283 \pm 308
ZD17	3660 \pm 11	469,369 \pm 9489	8.1 \pm 0.2	751.9 \pm 3.8	0.0628 \pm 0.0004	3972 \pm 25	689 \pm 470	753 \pm 4	668 \pm 470
ZD24	3759 \pm 13	669,952 \pm 13,565	7.9 \pm 0.2	746.7 \pm 3.9	0.0851 \pm 0.0005	5430 \pm 36	830 \pm 660	748 \pm 4	809 \pm 660

$d^{234}\text{U} = ([^{234}\text{U}/^{238}\text{U}]_{\text{activity}} - 1) \times 1000$. $d^{234}\text{U}_{\text{initial}}$ was calculated based on ^{230}Th age (T), i.e., $d^{234}\text{U}_{\text{initial}} = d^{234}\text{U}_{\text{measured}} \times e^{\lambda^{234} \times T}$. Corrected ^{230}Th ages assume the initial $^{230}\text{Th}/^{232}\text{Th}$ atomic ratio of $6.7 \pm 0.67 \times 10^{-6}$. Those are the values for the modern lake water. The errors are arbitrarily assumed to be 10%. B.P. stands for “Before Present”, where the “Present” is defined as the year 2000 AD.

The trend line formula was used to calculate the ages at 0 mm of travertine section. Combined with the measured ages of ZD10, ZD17, and ZD24, the deposition rate of each section was calculated (2.4–4.4 mm/yr). The ages of other samples were obtained by linear interpolation (Figure 3).

4.2. Petrography and Mineralogy

Among the travertine lithotypes proposed by Guo and Riding [51], the crystalline crust was recognized in Zabuye Salt Lake travertine. The travertine was formed from abiotic feather dendrite, radiating dendrite, micrite, and intraclast (Figure 4). The inner clasts are composed of travertine clasts, quartz, and feldspar grains. Travertine stratification is good, with overall density and few voids. The interaction between micrite and microsparry is more reflective of the difference in water environment. The formation of sparry calcite was under hydrodynamic conditions of high flow velocity, and the formation of micrite calcite was under hydrodynamic condition of low flow velocity.

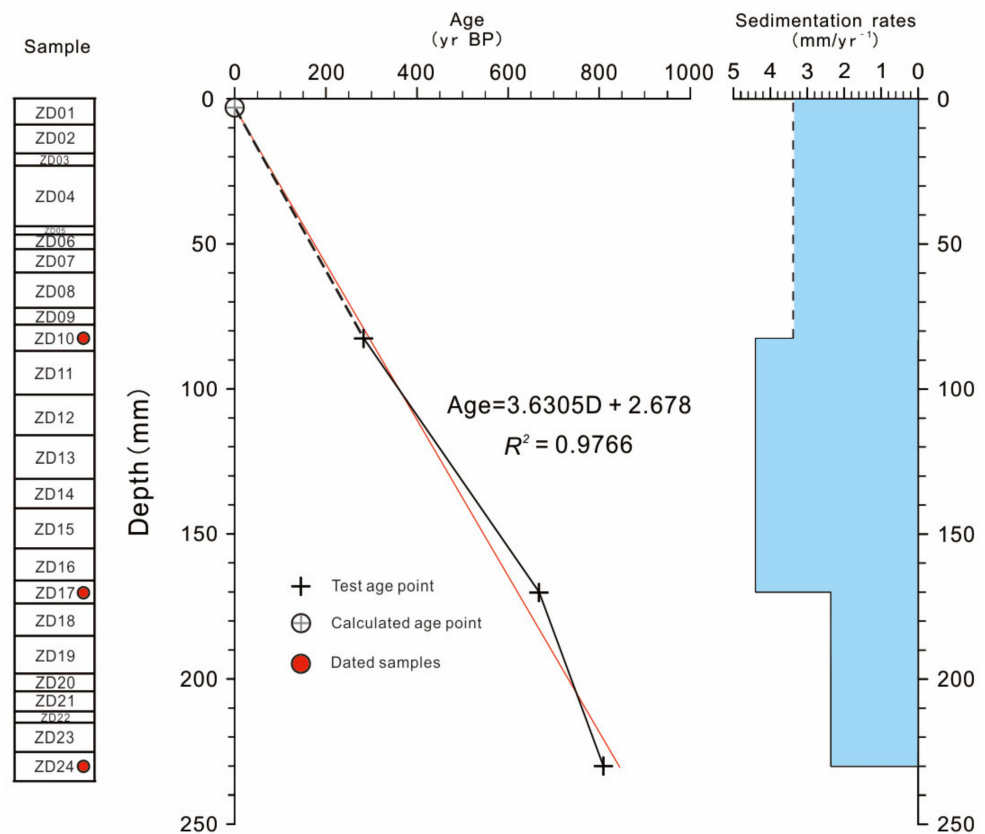


Figure 3. Age-depth profile based on U–Th dating from Zabuye Salt Lake travertine dam. The dotted lines represent the value calculated using the age formula.

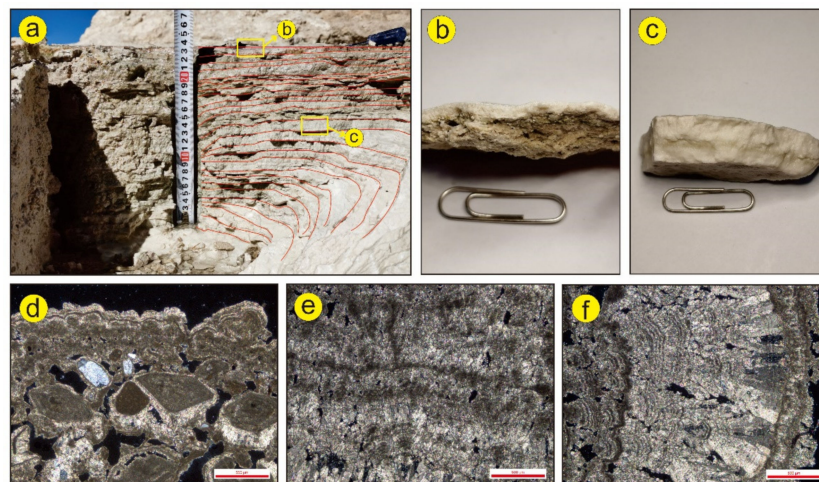


Figure 4. Textures of travertine of Zabuye Salt Lake. (a) Travertine profile with good stratification. (b) Sample at top of profile (ZD01) with higher porosity. (c) Dense middle section sample (ZD12). (d) Clastic nuclei are composed of travertine clasts, quartz, and feldspar grains. (e) Generation growth relationship exists between base of microsparry and micrite. (f) Crystalline dendrite textures showing wavy and banded internal zonations. The length of the red line segment is 500 μm .

XRD analysis of 24 samples shows that the mineral composition of the travertine profile is simple, mainly calcite, and some samples contain a small amount of quartz and feldspar. The calcite content ranges from 95.2% to 100%, with an average of 98.3%. Quartz content varies from 0.5% to 3.8%, with an average of 1.6%. Feldspar content ranges from 0.5% to 1.6%, with an average of 1.2%; feldspar content is very low, and specific feldspar

species can no longer be distinguished. Quartz and feldspar are detrital mineral grains of rocks around the basin carried mainly by wind and rain. The presence of small amounts of authigenic quartz and feldspar also cannot be ruled out. The range of MgCO_3 content in calcite (mol%) in the travertine dam is 0.5 to 3.6%, with an average of 1.8%, all of which is LMC (Figure 5).

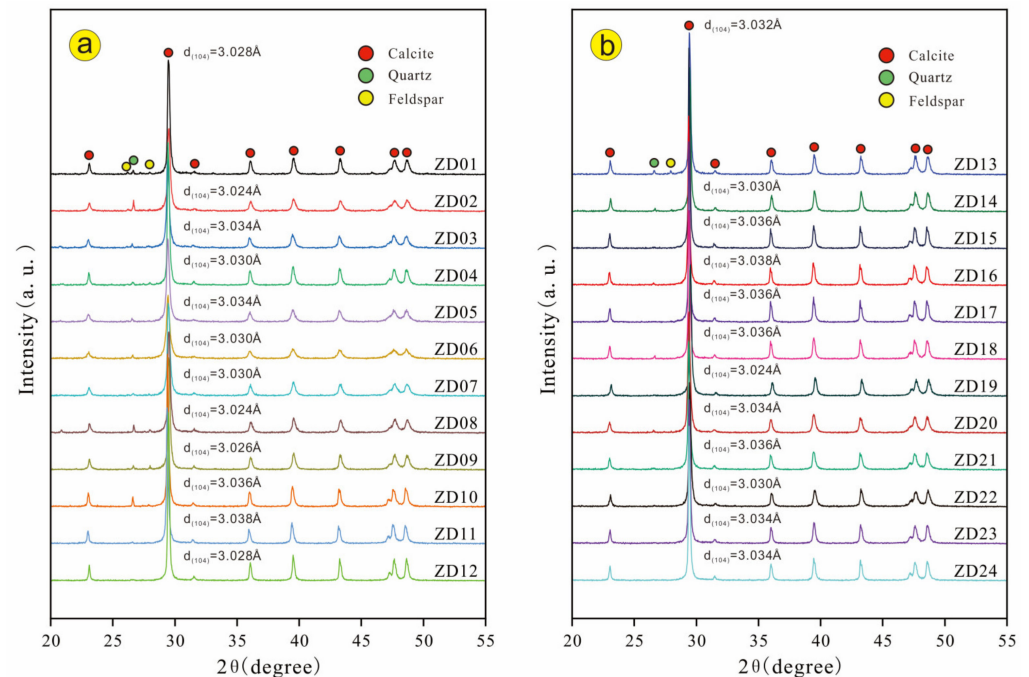


Figure 5. X-ray diffraction patterns of travertine samples. (a) X-ray diffraction patterns of samples ZD01–ZD12. (b) X-ray diffraction patterns of samples ZD13–ZD24.

Since the travertine dam is basically composed of calcite, the presence of aragonite and other calcium carbonate minerals was not observed, and the influence of the change of carbonate mineral facies on the change of carbon and oxygen isotopes of travertine can be excluded.

4.3. Hydrogen and Oxygen Isotopes of the Water Samples

Two spring samples (ZQ01–02) and one lake water sample (ZH01) were used for hydrogen and oxygen isotope analysis. The $\delta\text{D}_{\text{V-SMOW}}$ values ranged from 12.5‰ to 15.9‰, $\delta^{18}\text{O}_{\text{V-SMOW}}$ from -118.9 ‰ to -136.6 ‰ (Table 2). Craig first found a linear correlation between δD and $\delta^{18}\text{O}$ in atmospheric precipitation: $\delta\text{D} = 8\delta^{18}\text{O} + 10$ [52,53], which is also called the global meteoric water line (GMWL) on the graph of the relationship between δD and $\delta^{18}\text{O}$. The δD and $\delta^{18}\text{O}$ test data of the three water samples collected were combined with the δD and $\delta^{18}\text{O}$ data of the two spring waters samples of the travertine island [43] to draw the δD – $\delta^{18}\text{O}$ diagram (Figure 6). It can be seen that for the GMWL, the data of the sampling point have a slight ^{18}O drift, but it is not far from the GMWL, indicating that the hot groundwater comes from atmospheric precipitation but has a certain ^{18}O exchange with rocks and minerals during the deep cycle.

Table 2. Hydrogen and oxygen isotope data of Zabuye water samples.

Sample	$\delta\text{D}_{\text{V-SMOW}}$ (‰)	$\delta^{18}\text{O}_{\text{V-SMOW}}$ (‰)
ZQ-01	−132.9	−14.5
ZQ-02	−136.6	−15.9
ZH-01	−118.9	−12.8

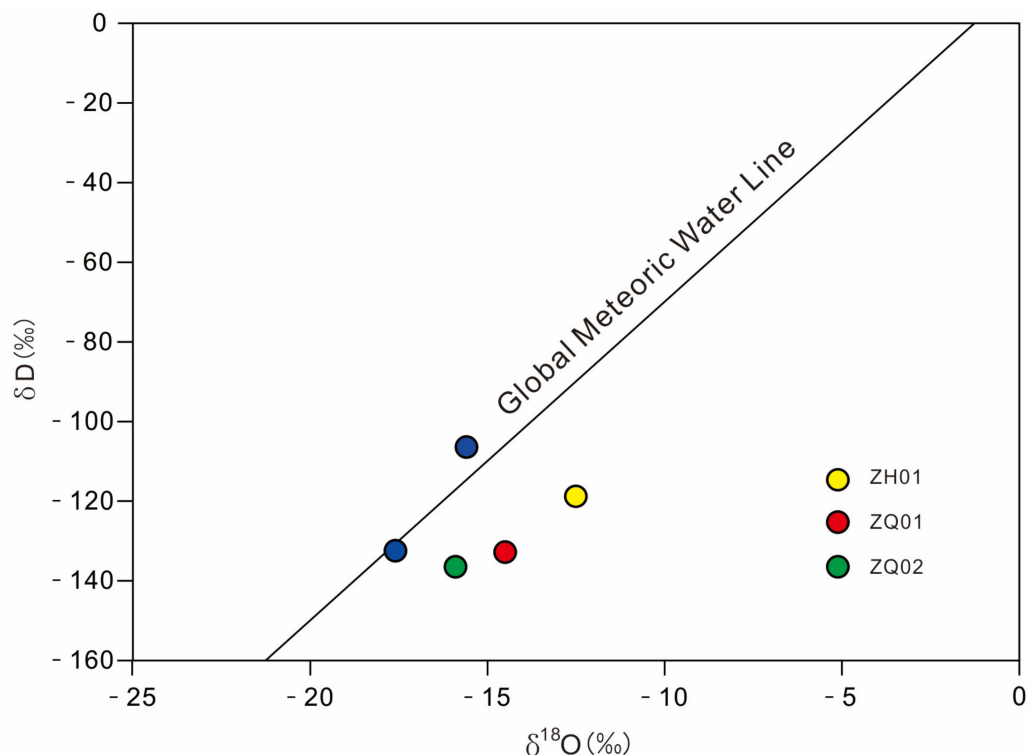


Figure 6. Plot of δD - $\delta^{18}O$ of Zabuye spring samples. Blue dot indicates data from [43].

4.4. Carbon and Oxygen Isotopes

Twenty-four travertine samples were used for carbon and oxygen isotope testing. $\delta^{13}C_{V-PDB}$ values ranged from 0.5‰ to 2.6‰, with an average of 1.0‰, and $\delta^{18}O$ values ranged from -12.4 ‰ to -6.4 ‰, with an average value of -10.3 ‰. There is a good correlation between $\delta^{18}O$ and $\delta^{13}C$ ($r = 0.92$). All carbon isotope data of travertine are within the range of thermogenic travertine.

The $\delta^{13}C$ value of travertine can be used to calculate the carbon isotopic composition of the parent CO_2 gas, using the empirical equation: $\delta^{13}C_{CO_2} = 1.2 \times \delta^{13}C_{travertine} - 10.5$ [54]. Applying this equation to the carbon isotope data of the travertine dam, the obtained $\delta^{13}C_{CO_2}$ values ranged from -9.9 ‰ to -7.4 ‰, with an average of -9.3 ‰.

There are three major CO_2 sources for travertine: soil, magma, and limestone decarbonation [39]. The $\delta^{13}C$ of soil CO_2 is controlled by the predominant vegetation type in the region. Globally, the $\delta^{13}C$ of C3 plants varies from -37 ‰ to -20 ‰, with an average of -28.7 ‰ [55]; the $\delta^{13}C$ of C4 plants varies from -15 ‰ to -9 ‰, with an average of -13 ‰ [56]. The $\delta^{13}C$ of CO_2 from the mantle generally ranges from -8 ‰ to -3 ‰ [57] or from the $\delta^{13}C$ of magmatic CO_2 generally ranges from -7 ‰ to -5 ‰ [58]. The $\delta^{13}C$ of CO_2 from typical limestone metamorphic sources is -1 ‰ to 2 ‰ [59]. Comparing the carbon and oxygen isotopes to the data [60] indicates that the CO_2 originated from carbonates or igneous rocks (Figure 7).

Based on the above analysis and taking into account that C4 plants are scarce in high-elevation regions [61], according to the current data, it is suggested that the parent CO_2 of the travertine dam mainly originated from thermal decarbonation of carbonates and intermediate–basic volcanic rocks around the basin, partly from magmatic mantle degassing and soil CO_2 . The fault system developed in the Zabuye Salt Lake area, and soil CO_2 in the basin was transferred into the groundwater cycle through atmospheric precipitation and mixed with CO_2 from deep underground sources. Since the $\delta^{13}C$ of soil CO_2 is obviously negative, even a small change in soil CO_2 will cause obvious changes to $\delta^{13}C$ in travertine.

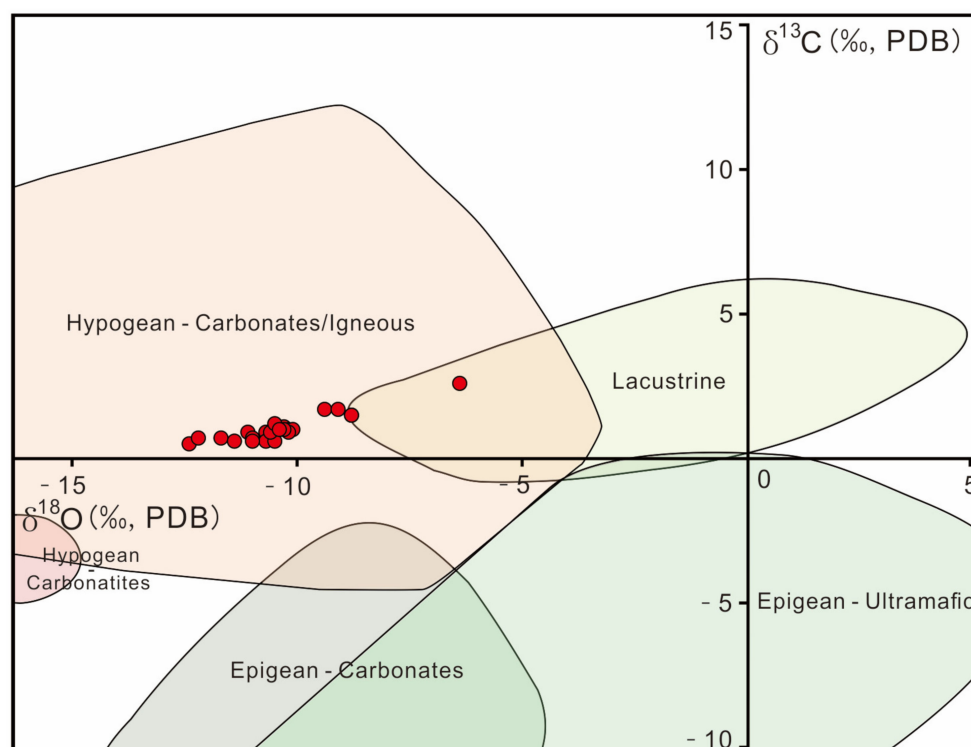


Figure 7. Results of stable isotopes overlain on clusters. All dots plotted within hypogean travertine area of Teboul et al. [60], with CO₂ derived from carbonates or an igneous source.

5. Discussion

5.1. Paleoclimatic Implications

The premise of travertine deposition is flowing water rich in dissolved CO₂ [62]. When high pCO₂ groundwater discharges from the spring, due to the low atmospheric pCO₂, CO₂ will be degassed rapidly, resulting in oversaturation of calcite, then calcite precipitation [63]. Travertine deposits can retain geochemical characteristics inherited from the parent fluid, so it is considered to be a favorable object for reconstructing paleoclimate and paleofluid characteristics [64].

Travertine is a comprehensive product of interactions between underground materials (mantle-derived carbon dioxide, magmatic water, surrounding rocks involved in groundwater circulation), atmospheric precipitation, and surface materials (soil carbon dioxide, major and trace elements). The information carried by travertine can reflect surface information when the subsurface material remains basically unchanged. That is, when the magmatic and tectonic activities in a certain area are stable, the area maintains relatively stable hydrothermal activity. The travertine formed against this background is relatively stable under the influence of mantle-derived CO₂ and CO₂ and magmatic water formed by decarbonization of surrounding carbonate rocks. The carbon and oxygen isotope change in travertine is less affected by the above, but more controlled by the change in soil CO₂ supply and atmospheric precipitation, which are directly affected by climatic factors. The amount of groundwater infiltration by atmospheric precipitation is directly related to the rainfall in the region, the soil CO₂ is related to the type and density of vegetation in the region, and the climatic conditions determine the vegetation.

Studies based on the hydrogen and oxygen isotopes of geothermal spring water indicate that geothermal springs are mainly supplied by meteoric precipitation and water from melted glaciers/ice, and most geothermal spring water circulates rapidly deep underground with a cycle time of only 20–40 years [65–67]. The Zabuye Salt Lake area is structurally stable, and no earthquakes of magnitude 5 or greater have been recorded [68]. The average age of travertine samples from the edge stone dam of the lake is about 33 yr.

From the perspective of chronology, travertine can reflect the geological information carried by atmospheric precipitation in the water cycle process in this region.

The $\delta^{13}\text{C}$ and $\delta^{18}\text{O}$ of travertine show an obvious positive correlation ($r = 0.922$), indicating that the two are affected by the same or similar factors. In a continuous high-resolution (monthly) study of stable isotopes of $\delta^{13}\text{C}$ and $\delta^{18}\text{O}$ in travertine in Baishuitai, there is a strong correlation between carbon and oxygen isotopes ($r = 0.75$); Liu et al. believe that rainwater is the main factor causing the seasonal variation of $\delta^{13}\text{C}$ and $\delta^{18}\text{O}$ [69]. This indicates that $\delta^{13}\text{C}$ and $\delta^{18}\text{O}$ of the Zabuye Salt Lake travertine dam can reflect changes in the surface climate environmental system.

Under the condition of relatively stable tectonic movement, CO_2 from deep sources and the hydro-rock interaction of hot springs are relatively fixed. In arid climates, it is difficult to form a suitable plant cover, while in humid climates, $\delta^{13}\text{C}$ in travertine shifts to negative values when biomass develops more [70]. The $\delta^{18}\text{O}_{\text{H}_2\text{O}}$ value of hot springs depends on the $\delta^{18}\text{O}$ value of atmospheric precipitation. Because the temperature of Zabuye spring is stable and less affected by air temperature [43] and the travertine dam is located only a few meters from the spring hole (Figure 2), the effect of water temperature change on its $\delta^{18}\text{O}$ during the deposition of travertine is negligible. Therefore, the variation of $\delta^{18}\text{O}$ of Zabuye Salt Lake travertine dam can reflect the variation of $\delta^{18}\text{O}$ of atmospheric precipitation.

In the transition region between the westerlies and Indian summer monsoon (30°N – 35°N) over the Tibetan Plateau, the factors that influence atmospheric precipitation isotope change are complex and are sensitive to the water vapor source and transport process [71]. In this region, the $\delta^{18}\text{O}$ in precipitation formed by water vapor from Indian summer monsoon entering the southern plateau is lower, and the stronger monsoon activity lowers the $\delta^{18}\text{O}$ in precipitation. The $\delta^{18}\text{O}$ values of water vapor from the northern Tibetan Plateau and precipitation formed by local evaporation water vapor are higher [71–73].

Based on the above discussion, in this paper we believe that the $\delta^{13}\text{C}$ of travertine dam can be used as an index of precipitation change: lighter (heavier) $\delta^{13}\text{C}$ indicates increased (decreased) precipitation; $\delta^{18}\text{O}$ mainly indicates variations of monsoon intensity and water vapor source, and lighter (heavier) $\delta^{18}\text{O}$ indicates increased (decreased) Indian summer monsoon precipitation.

5.2. Precipitation Changes at Zabuye Salt Lake over the Past 800 Years

With the exception of a warm period in the 20th century, which occurred simultaneously all over the globe, the changes in warm and cold phases around the world before the Industrial Revolution were not synchronized. Based on previous research results [74–77], in this paper we roughly divide the temperature stages of the Tibetan Plateau over the past thousand years into the Medieval Warm Period (MWP, 800–1400 AD), Little Ice Age (LIA, 1400–1900 AD), and Current Warm Period (CWP, 1900–2000 AD).

Based on the changes in $\delta^{13}\text{C}$ and $\delta^{18}\text{O}$ of travertine in this study, we reconstructed the precipitation records of Zabuye Salt Lake over the past 800 years (1191–1982 AD). The results show a dry condition in 1191–1374 AD (MWP), a humid condition in 1374–1884 AD (LIA), and a dry condition in 1884–1982 AD (CWP), indicating a warm–dry/cold–moist climate pattern (Figure 8). Zhang et al. [74] studied climate change over the past 300 years at Taro Co, 10 km south of Zabuye Salt Lake (Figure 1c), and showed that the climate was humid during 1750–1860 AD and was dry from 1860 AD to the present [78], which is consistent with our reconstruction results.

We compared the precipitation records of Zabuye with other typical precipitation records of the Tibetan Plateau (Figures 1b and 8), including the accumulated records of the Guliya glacier in the northwestern part of the plateau [41], annual mean precipitation based on quantitative pollen reconstruction at Yamzhog Yumco Lake in the southern part of the plateau (MAP) [11], precipitation records reconstructed from tree rings in Linzhou [7], and June to September (JJAS) precipitation based on grain size reconstruction in Ngamring Tso [13]. These records are very similar to the precipitation records of Zabuye Salt Lake, and are also characterized by a warm–dry/cold–moist pattern. In addition, Lugu Lake [79] and

Erhai Lake [80], which are subjected to seasonal risk control in the southeast of the Tibetan Plateau, both showed warm–dry/cold–moist climate characteristics in the MWP/LIA. This climatic pattern appeared not only in areas controlled by the westerlies, but also in wider areas controlled by Indian summer monsoon. In southern Oman, the stalagmite $\delta^{18}\text{O}$ record from Qunf Cave shows higher values during the MWP than the LIA, indicating a weakening of Indian summer monsoon intensity during the MWP [81]. Over the past 100–200 years, the Indian summer monsoon has gradually decreased in intensity, and the climate has become drier under warmer conditions [82–84]. In the entire monsoon region, the climate conditions during the MWP and the past 100–200 years were significantly dry and during the LIA were relatively humid, and this pattern was prevalent [79].

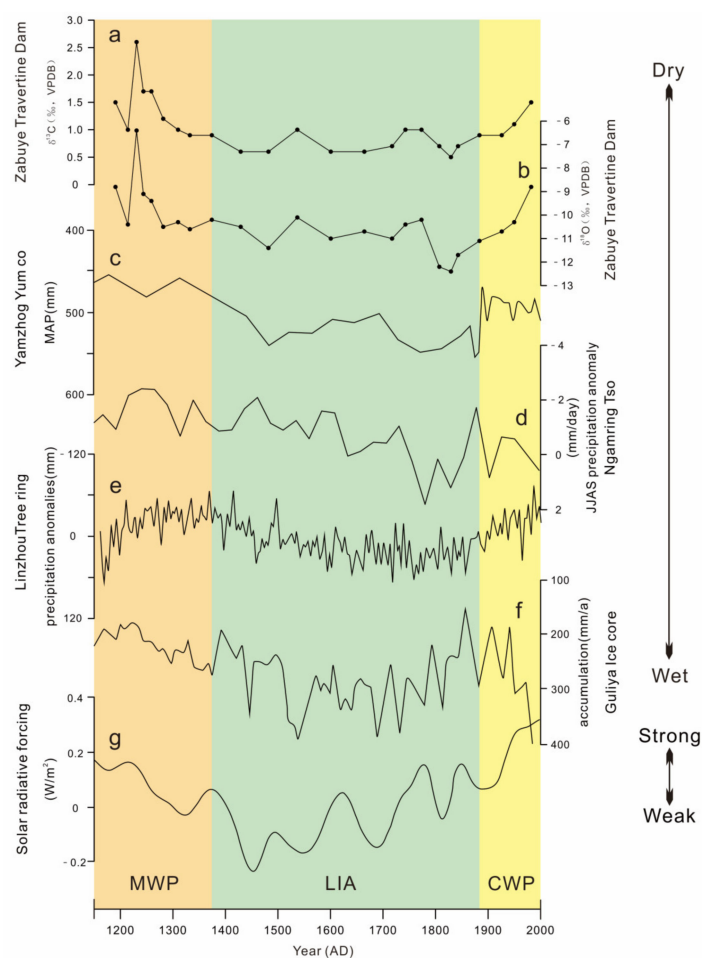


Figure 8. Comparison of climatic records from Zabuye Salt Lake travertine dam with other climatic records. (a) Carbon isotopes of carbonate of travertine dam. (b) Oxygen isotopes of carbonate. (c) Mean annual precipitation (MAP) at Yamzhog Yumco Lake [11]. (d) June to September (JJAS) precipitation at Ngamring Tso [13]. (e) Tree ring precipitation anomalies at Linzhou [7]. (f) Ice core accumulation at Guliya [41]. (g) Solar radiative forcing [85]. MWP, LIA, and CWP refer to Medieval Warm Period, Little Ice Age, and Current Warm Period, respectively.

Monsoons and westerlies interact with each other over the Tibetan Plateau at glacial–interglacial, millennial, decadal, and seasonal scales, bringing water vapor to different areas of the plateau [86]. Although the climate characteristics of warm–dry, cold–wet in the Zabuye Salt Lake area are similar to those recorded in the Guliya ice core, the oxygen isotopes of travertine become lighter in humid periods (LIA) and heavier in dry periods (MWP and CWP) (Figure 8a,b), indicating that climate change in the Zabuye Salt Lake area in the past 800 years has mainly been controlled by the influence of the Indian summer monsoon. In addition, the temperature change driven by solar radiation will lead to a

change in evaporation intensity, and then affect the dry and wet climate change of the Tibetan Plateau [11]. The precipitation records for the Zabuye Salt Lake area are consistent with the solar radiation (Figure 8g). This study argues that during the MWP, the Zabuye Salt Lake region had higher temperatures, strong evaporation, and less precipitation, resulting in an arid climate during this period; during the LIA, the temperature was low, evaporation was inhibited, and there was more precipitation, so the climate was humid.

6. Conclusions

Based on U–Th dating of a travertine dam, this study establishes the chronology of Zabuye Salt Lake travertine over the past 800 years, preliminarily discusses the carbon and oxygen isotopes of travertine as a precipitation index, and points out that travertine might record the evolution of paleoprecipitation (paleomonsoon) on at least a decadal–centennial scale. The precipitation records of Zabuye Salt Lake over the past 800 years show a dry condition in 1191–1374 AD (MWP), a humid condition in 1374–1884 AD (LIA), and a dry condition in 1884–1982 AD (CWP), indicating a warm–dry/cold–moist climate pattern. The Indian summer monsoon has been the main factor influencing precipitation change at Zabuye Salt Lake over the past 800 years, and the change in evapotranspiration intensity caused by temperature change driven by solar radiation is also an important factor affecting the dry–moist change. It should be pointed out that our precipitation reconstruction index is relatively single and lacks evidence from other proxy indices. Whether the westerlies have an influence and to what extent still needs further study.

Author Contributions: Conceptualization, M.L. and M.Z.; methodology, M.L., M.Z. and C.Y.; software, M.L. and X.W.; validation, M.L. and M.Z.; formal analysis, M.L., X.W. and Y.Z. (Yuanyi Zhao); investigation, M.L., C.Y., X.Z. and Y.Z. (Yuanyi Zhao); resources, M.Z.; data curation, M.Z.; writing—original draft preparation, M.L. and M.Z.; writing—review and editing, M.L., M.Z., C.Y., C.W., X.Z. and Y.Z. (Yanbo Zhang); visualization, M.L. and C.Y.; supervision, M.Z.; project administration, M.Z.; funding acquisition, M.Z. All authors have read and agreed to the published version of the manuscript.

Funding: This work was supported by the National Natural Science Foundation of China (No: 91962219, 41673023).

Data Availability Statement: Not applicable.

Acknowledgments: We thank the anonymous reviewers whose comments have improved the quality of the manuscript.

Conflicts of Interest: The authors declare no conflict of interest.

References

1. Qiu, J. China: The third pole. *Nature* **2008**, *454*, 393–396. [[PubMed](#)]
2. Yao, T.; Thompson, L.G.; Mosbrugger, V.; Zhang, F.; Ma, Y.; Luo, T.; Xu, B.; Yang, X.; Joswiak, D.R.; Wang, W.; et al. Third Pole Environment (TPE). *Environ. Dev.* **2012**, *3*, 52–64.
3. Liu, X.; Zheng, H.; Zhang, M.; Liu, C. Identification of dominant climate factor for pan evaporation trend in the Tibetan Plateau. *J. Geogr. Sci.* **2011**, *21*, 594–608.
4. Flantua, S.; Henry, H.; Vuille, M.; Carson, J.; Gosling, W.; Hoyos, I.; Ledru, M.-P.; Montoya, E.; Mayle, F.; Maldonado, A.; et al. Climate variability and human impact in South America during the last 2000 years: Synthesis and perspectives from pollen records. *Clim. Past* **2016**, *12*, 483–523.
5. Shao, X.; Xu, Y.; Yin, Z.Y.; Liang, E.; Zhu, H.; Wang, S. Climatic implications of a 3585-year tree-ring width chronology from the northeastern Qinghai-Tibetan Plateau. *Quat. Sci. Rev.* **2010**, *29*, 2111–2122. [[CrossRef](#)]
6. Yang, B.; Qin, C.; Wang, J.; He, M.; Melvin, T.M.; Osborn, T.J.; Briffa, K.R. A 3500-year tree-ring record of annual precipitation on the northeastern Tibetan Plateau. *Proc. Natl. Acad. Sci. USA* **2014**, *111*, 2903–2908.
7. He, M.; Yang, B.; Wang, J.; Wang, Z. Tree-ring-derived millennial precipitation record for the southern Tibetan Plateau and its possible driving mechanism. *Holocene* **2013**, *23*, 36–45.
8. Griesinger, J.; Bräuning, A.; Helle, G.; Thomas, A.; Schleser, G. Late Holocene Asian summer monsoon variability reflected by $\delta^{18}\text{O}$ in tree-rings from Tibetan junipers. *Geophys. Res. Lett.* **2011**, *38*, L03701. [[CrossRef](#)]
9. Yao, T.; Duan, K.; Xu, B.; Wang, N.; Guo, X.; Yang, X. Precipitation record since AD 1600 from ice cores on the central Tibetan Plateau. *Clim. Past* **2008**, *4*, 175–180.

10. Pang, H.; Hou, S.; Zhang, W.; Wu, S.; Jenk, T.M.; Schwikowski, M.; Jouzel, J. Temperature Trends in the Northwestern Tibetan Plateau Constrained by Ice Core Water Isotopes Over the Past 7000 Years. *J. Geophys. Res. Atmos.* **2020**, *125*, e2020JD032560.
11. Guo, C.; Ma, Y.; Meng, H.; Hu, C.; Li, D.; Liu, J.; Luo, C.; Wang, K. Changes in vegetation and environment in Yamzhog Yumco Lake on the southern Tibetan Plateau over past 2000 years. *Palaeogeogr. Palaeoclim. Palaeoecol.* **2018**, *501*, 30–44. [[CrossRef](#)]
12. He, Y.; Zhao, C.; Wang, Z.; Wang, H.; Song, M.; Liu, W.; Liu, Z. Late Holocene coupled moisture and temperature changes on the northern Tibetan Plateau. *Quat. Sci. Rev.* **2013**, *80*, 47–57.
13. Conroy, J.L.; Hudson, A.M.; Overpeck, J.T.; Liu, K.-B.; Wang, L.; Cole, J.E. The primacy of multidecadal to centennial variability over late-Holocene forced change of the Asian Monsoon on the southern Tibetan Plateau. *Earth Planet. Sci. Lett.* **2017**, *458*, 337–348.
14. Li, X.; Liang, J.; Hou, J.; Zhang, W. Centennial-scale climate variability during the past 2000 years on the central Tibetan Plateau. *Holocene* **2015**, *25*, 892–899. [[CrossRef](#)]
15. Ji, K.; Zhu, E.; Chu, G.; Aquino-López, M.A.; Hou, J. A record of late Holocene precipitation on the Central Tibetan Plateau inferred from varved lake sediments. *J. Paleolimnol.* **2021**, *66*, 439–452. [[CrossRef](#)]
16. Hou, J.; D'Andrea, W.J.; Liu, Z. The influence of ¹⁴C reservoir age on interpretation of paleolimnological records from the Tibetan Plateau. *Quat. Sci. Rev.* **2012**, *48*, 67–79.
17. Wang, Z.; Yin, J.-J.; Cheng, H.; Ning, Y.; Meyer, M.C. Climatic controls on travertine deposition in southern Tibet during the late Quaternary. *Palaeogeogr. Palaeoclim. Palaeoecol.* **2022**, *589*, 110852. [[CrossRef](#)]
18. Viles, H.A.; Tufas, A.G. Travertines and allied carbonate deposits. *Prog. Phys. Geogr.* **1990**, *14*, 19–41. [[CrossRef](#)]
19. Ford, T.; Pedley, H. A review of tufa and travertine deposits of the world. *Earth-Sci. Rev.* **1996**, *41*, 117–175.
20. Pentecost, A.; Viles, H. A Review and Reassessment of Travertine Classification. *Geogr. Phys. Quat.* **1994**, *48*, 305–314.
21. Capezzuoli, E.; Gandin, A.; Pedley, M. Decoding tufa and travertine (fresh water carbonates) in the sedimentary record: The state of the art. *Sedimentology* **2014**, *61*, 1–21.
22. Pentecost, A. The quaternary travertine deposits of Europe and Asia Minor. *Quat. Sci. Rev.* **1995**, *14*, 1005–1028.
23. Agliasacchi, E.; Kayseri-Özer, M.S. Multidisciplinary approach for palaeoclimatic signals of the non-marine carbonates: The case of the Sarikavak tufa deposits (Afyon, SW-Turkey). *Quat. Int.* **2019**, *544*, 41–56.
24. Andrews, J.E.; Brasier, A. Seasonal records of climatic change in annually laminated tufas: Short review and future prospects. *J. Quat. Sci.* **2005**, *20*, 411–421.
25. Andrews, J. Palaeoclimatic records from stable isotopes in riverine tufas: Synthesis and review. *Earth-Sci. Rev.* **2006**, *75*, 85–104.
26. Kano, A.; Kawai, T.; Matsuoka, J.; Ihara, T. High-resolution records of rainfall events from clay bands in tufa. *Geology* **2004**, *32*, 793.
27. Toker, E.; Kayseri-Özer, M.S.; Özkul, M.; Kele, S.; Ariztegui, D. Depositional system and palaeoclimatic interpretations of Middle to Late Pleistocene travertines: Kocabaş, Denizli, south-west Turkey. *Sedimentology* **2015**, *62*, 1360–1383.
28. De Filippis, L.; Faccenna, C.; Billi, A.; Anzalone, E.; Brilli, M.; Soligo, M.; Tuccimei, P. Plateau versus fissure ridge travertines from Quaternary geothermal springs of Italy and Turkey: Interactions and feedbacks between fluid discharge, paleoclimate, and tectonics. *Earth-Sci. Rev.* **2013**, *123*, 35–52.
29. Rodríguez-Berriguete, Á.; Alonso-Zarza, A.M.; Martín-García, R.; Cabrera, M.d.C. Sedimentology and geochemistry of a human-induced tufa deposit: Implications for palaeoclimatic research. *Sedimentology* **2018**, *65*, 2253–2277.
30. Faccenna, C.; Soligo, M.; Billi, A.; De Filippis, L.; Funicello, R.; Rossetti, C.; Tuccimei, P. Late Pleistocene depositional cycles of the Lapis Tiburtinus travertine (Tivoli, Central Italy): Possible influence of climate and fault activity. *Glob. Planet. Chang.* **2008**, *63*, 299–308.
31. Ricketts, J.W.; Ma, L.; Wagler, A.E.; Garcia, V.H. Global travertine deposition modulated by oscillations in climate. *J. Quat. Sci.* **2019**, *34*, 558–568.
32. Su, J.; Tan, H.; Chen, X. The groundwater deep circulation and large-scale geothermal deposition in response to the extension of the Yadong–Gulu rift, South Tibet, China. *J. Volcanol. Geotherm. Res.* **2020**, *395*, 106836.
33. Wang, Z.; Meyer, M.C.; Hoffmann, D.L. Sedimentology, petrography and early diagenesis of a travertine–colluvium succession from Chusang (southern Tibet). *Sediment. Geol.* **2016**, *342*, 218–236.
34. Wang, Z.; Meyer, M.C.; Gliganic, L.A.; Hoffmann, D.L.; May, J.-H. Timing of fluvial terrace formation and concomitant travertine deposition in the upper Sutlej River (Tirthapuri, southwestern Tibet) and paleoclimatic implications. *Quat. Sci. Rev.* **2017**, *169*, 357–377.
35. Zentmyer, R.; Myrow, P.M.; Newell, D.L. Travertine deposits from along the South Tibetan Fault System near Nyalam, Tibet. *Geol. Mag.* **2008**, *145*, 753–765.
36. Gao, J.; Zhou, X.; Fang, B.; Li, T.; Tang, L. U-series dating of the travertine depositing near the Rongma hot springs in northern Tibet, China, and its paleoclimatic implication. *Quat. Int.* **2012**, *298*, 98–106.
37. Wang, Z.J.; Yin, J.; Yuan, D.X. Possibilities and problems associated with travertines and tufas in Quaternary studies: A case of the Tibetan Plateau. *Chin. Sci. Bull.* **2018**, *63*, 1012–1023, (In Chinese with English Abstract).
38. Hammer, Ø.; Dysthe, D.K.; Jamtveit, B. The dynamics of travertine dams. *Earth Planet. Sci. Lett.* **2007**, *256*, 258–263.
39. Pentecost, A.; Travertine, A. (Eds.) *Pentecost*; Springer: Dordrecht, The Netherlands, 2005; p. 446.
40. Ding, T.; Zheng, M.; Nie, Z.; Ma, L.; Ye, C.; Wu, Q.; Zhao, Y.; Yang, D.; Wang, K. Impact of Regional Climate Change on the Development of Lithium Resources in Zabuye Salt Lake, Tibet. *Front. Earth Sci.* **2022**, *10*, 865158.

41. Thompson, L.G.; Mosley-Thompson, E.; Davis, M.E.; Lin, P.N.; Dai, J.; Bolzan, J.F.; Yao, T. A 1000 year climate ice-core record from the Guliya ice cap, China: Its relationship to global climate variability. *Ann. Glaciol.* **1995**, *21*, 175–181.
42. Liu, X.F.; Zheng, M.P.; Qi, W. Sources of Ore-Forming Materials of the Superlarge B and Li Deposit in Zabuye Salt Lake, Tibet, China. *Acta Geol. Sin.* **2007**, *81*, 1709–1715, (In Chinese with English Abstract).
43. Zheng, M.P.; Xiang, J.; Wei, X.J.; Zheng, Y. *Saline Lake on the Qinghai-Xizang (Tibet) Plateau*; Science Press: Beijing, China, 1989; pp. 1–431, (In Chinese with English Abstract).
44. Cheng, H.; Lawrence Edwards, R.; Shen, C.-C.; Polyak, V.J.; Asmerom, Y.; Woodhead, J.; Hellstrom, J.; Wang, Y.; Kong, X.; Spötl, C.; et al. Improvements in ^{230}Th dating, ^{230}Th and ^{234}U half-life values, and U–Th isotopic measurements by multi-collector inductively coupled plasma mass spectrometry. *Earth Planet. Sci. Lett.* **2013**, *371–372*, 82–91.
45. Edwards, R.L.; Chen, J.; Wasserburg, G. $^{238}\text{U}/^{234}\text{U}/^{230}\text{Th}/^{232}\text{Th}$ systematics and the precise measurement of time over the past 500,000 years. *Earth Planet. Sci. Lett.* **1987**, *81*, 175–192.
46. Lumsden, D.N. Discrepancy Between Thin-Section and X-Ray Estimates of Dolomite in Limestone. *J. Sediment. Res.* **1979**, *49*, 429–435.
47. Goldsmith, J.R.; Graf, D.L.; Chodos, A.A.; Joensuu, O.I.; McVicker, L.D. Relation between lattice constants and composition of Ca-Mg carbonates. *Am. Mineral.* **1958**, *43*, 84–101.
48. Haese, R.R.; Smith, J.; Weber, R.; Trafford, J. High-Magnesium Calcite Dissolution in Tropical Continental Shelf Sediments Controlled by Ocean Acidification. *Environ. Sci. Technol.* **2014**, *48*, 8522–8528.
49. Auler, A.S.; Smart, P.L. Late Quaternary Paleoclimate in Semiarid Northeastern Brazil from U-Series Dating of Travertine and Water-Table Speleothems. *Quat. Res.* **2001**, *55*, 159–167.
50. Martínez-Aguirre, A.; Alcaraz-Pelegri, J.M.; Rodríguez-Vidal, J. U/Th dating of impure carbonates: $^{230}\text{Th}/^{232}\text{Th}$ activity ratios in detrital material. *J. Radioanal. Nucl. Chem. Artic.* **2019**, *321*, 71–81.
51. Guo, L.; Riding, R. Hot-spring travertine facies and sequences, Late Pleistocene, Rapolano Terme, Italy. *Sedimentology* **1998**, *45*, 163–180.
52. Craig, H. Isotopic Variations in Meteoric Waters. *Science* **1961**, *133*, 1702–1703.
53. Craig, H. Standard for Reporting Concentrations of Deuterium and Oxygen-18 in Natural Waters. *Science* **1961**, *133*, 1833–1834. [[PubMed](#)]
54. Panichi, C.; Tongiorgi, E. Carbon isotopic composition of CO_2 from springs, fumaroles, mofettes and travertines of central and southern Italy: A preliminary prospection method of geothermal areas. In Proceedings of the 2nd U.N. Symposium on the Development and Use of Geothermal Energy, San Francisco, CA, USA, 20–29 May 1975.
55. Kohn Matthew, J. Carbon isotope compositions of terrestrial C_3 plants as indicators of (paleo)ecology and (paleo)climate. *Proc. Natl. Acad. Sci. USA* **2010**, *107*, 19691–19695.
56. Wang, G.; Feng, X.; Han, J.; Lp, Z.; Wb, T.; Su, F. Paleovegetation reconstruction using $\delta^{13}\text{C}$ of Soil Organic Matter. *Biogeosciences* **2008**, *5*, 1325–1337.
57. Minissale, A.; Kerrick, D.M.; Magro, G.; Murrell, M.T.; Paladini, M.; Rihs, S.; Sturchio, N.C.; Tassi, F.; Vaselli, O. Geochemistry of Quaternary travertines in the region north of Rome (Italy): Structural, hydrologic and paleoclimatic implications. *Earth Planet. Sci. Lett.* **2002**, *203*, 709–728.
58. Hoefs, J. *Stable Isotope Geochemistry*; Springer: Berlin/Heidelberg, Germany, 1997; p. 201.
59. Rollinson, H.R. *Using Geochemical Data: Evaluation, Presentation, Interpretation. Mineralogical Magazine*; Longman Scientific and Technical: London, UK, 1993; Volume 58, 352p.
60. Teboul, P.A.; Durllet, C.; Gaucher, E.C.; Virgone, A.; Girard, J.P.; Curie, J.; Lopez, B.; Camoin, G.F. Origins of elements building travertine and tufa: New perspectives provided by isotopic and geochemical tracers. *Sediment. Geol.* **2016**, *334*, 97–114.
61. Boom, A.; Mora, G.; Cleef, A.M.; Hooghiemstra, H. High altitude C_4 grasslands in the northern Andes: Relicts from glacial conditions? *Rev. Palaeobot. Palynol.* **2001**, *115*, 147–160.
62. Rodrigo-Naharro, J.; Herrero, M.J.; Delgado-Huertas, A.; Granados, A.; Pérez del Villar, L. Current travertines precipitation related to artificial CO_2 leakages from a natural reservoir (Gañuelas-Mazarrón Tertiary Basin, SE Spain). *J. Hydrol.* **2019**, *577*, 123997.
63. Mancini, A.; Frondini, F.; Capezzuoli, E.; Mejia, E.G.; Lezzi, G.; Matarazzi, D.; Brogi, A.; Swennen, R. Evaluating the geogenic CO_2 flux from geothermal areas by analysing quaternary travertine masses. New data from western central Italy and review of previous CO_2 flux data. *Quat. Sci. Rev.* **2019**, *215*, 132–143.
64. Kokh, S.N.; Shnyukov, Y.F.; Sokol, E.V.; Novikova, S.A.; Kozmenko, O.A.; Semenova, D.V.; Rybak, E.N. Heavy carbon travertine related to methane generation: A case study of the Big Tarkhan cold spring, Kerch Peninsula, Crimea. *Sediment. Geol.* **2015**, *325*, 26–40.
65. Fang, B.; Yang, Y.J.; Wang, G.H.; Zhou, X.; Chen, S.N. Characteristics and resource evaluation of the Jiwa geothermal field in central Qiangtang, northern Tibet, China. *Geol. Bull. China* **2009**, *28*, 1335–1341, (In Chinese with English Abstract).
66. Zhou, L. Characteristics of the Typical Hot Springs in the Central Tibet. Master’s Thesis, China University of Geosciences (Beijing), Beijing, China, 2012. (In Chinese with English Abstract).
67. Chen, C.J. Provenance Analysis of Xiqin Geothermal Field, in Lazi County, Tibet. Master’s Thesis, Hebei GEO University, Shijiazhuang, China, 2019.

68. Chevalier, M.L.; Tapponnier, P.; Woerd, J.; Leloup, P.H.; Wang, S.; Pan, J.; Bai, M.; Kali, E.; Liu, X.; Li, H. Late Quaternary Extension Rates Across the Northern Half of the Yadong-Gulu Rift: Implication for East-West Extension in Southern Tibet. *J. Geophys. Res. Solid Earth* **2020**, *125*, e2019JB019106.
69. Liu, Z.; Li, H.; You, C.; Wan, N.; Sun, H. Thickness and stable isotopic characteristics of modern seasonal climate-controlled sub-annual travertine laminas in a travertine-depositing stream at Baishuitai, SW China: Implications for paleoclimate reconstruction. *Environ. Earth Sci.* **2006**, *51*, 257–265. [[CrossRef](#)]
70. Prado-Pérez, A.J.; Delgado Huertas, A.; Crespo, M.; SÁNchez, A.; Villar, L. Late Pleistocene and Holocene mid-latitude palaeoclimatic and palaeoenvironmental reconstruction: An approach based on the isotopic record from a travertine formation in the Guadix-Baza basin, Spain. *Geol. Mag.* **2013**, *150*, 602–625.
71. Yao, T.; Masson-Delmotte, V.; Gao, J.; Yu, W.; Yang, X.; Risi, C.; Sturm, C.; Werner, M.; Zhao, H.; He, Y.; et al. A review of climatic controls on $\delta^{18}\text{O}$ in precipitation over the Tibetan Plateau: Observations and simulations. *Rev. Geophys.* **2013**, *51*, 525–548.
72. Tian, L.; Yao, T.; Numaguti, A.; Sun, W. Stable Isotope Variations in Monsoon Precipitation on the Tibetan Plateau. *J. Meteorol. Soc. Jpn. Ser. II* **2001**, *79*, 959–966. [[CrossRef](#)]
73. Yu, W.; Yao, T.; Tian, L.; Ma, Y.; Ichiyanaagi, K.; Wang, Y.; Sun, W. Relationships between $\delta^{18}\text{O}$ in precipitation and air temperature and moisture origin on a south–north transect of the Tibetan Plateau. *Atmos. Res.* **2008**, *87*, 158–169. [[CrossRef](#)]
74. Feng, X.; Zhao, C.; D’Andrea, W.J.; Liang, J.; Zhou, A.; Shen, J. Temperature fluctuations during the Common Era in subtropical southwestern China inferred from brGDGTs in a remote alpine lake. *Earth Planet. Sci. Lett.* **2019**, *510*, 26–36.
75. Ge, Q.; Hao, Z.; Zheng, J.; Shao, X. Temperature changes over the past 2000 yr in China and comparison with the Northern Hemisphere. *Clim. Past* **2013**, *9*, 1153–1160. [[CrossRef](#)]
76. Bao, Y.; Braüning, A.; Yafeng, S. Late Holocene temperature fluctuations on the Tibetan Plateau. *Quat. Sci. Rev.* **2003**, *22*, 2335–2344. [[CrossRef](#)]
77. Li, X.; Zhang, Y.; Wang, M.; Yan, J.; Fan, B.; Xing, W.; He, Y.; Hou, J. Centennial-Scale Temperature Change During the Common Era Revealed by Quantitative Temperature Reconstructions on the Tibetan Plateau. *Front. Earth Sci.* **2020**, *8*, 360. [[CrossRef](#)]
78. Zhang, X.L.; Xu, B.Q.; Li, J.L.; Xi, Y.; Gao, S.P.; Wang, M. Climatic and environmental changes over the past about 300 years recorded by lake sediments in Taro Co, southwestern Tibetan Plateau. *J. Earth Sci. Environ.* **2012**, *34*, 79–90, (In Chinese with English Abstract).
79. Sheng, E.; Yu, K.; Xu, H.; Lan, J.; Liu, B.; Che, S. Late Holocene Indian summer monsoon precipitation history at Lake Lugu, northwestern Yunnan Province, southwestern China. *Palaeogeogr. Palaeoclim. Palaeoecol.* **2015**, *438*, 24–33. [[CrossRef](#)]
80. Xu, H.; Zhou, X.; Lan, J.; Liu, B.; Sheng, E.; Yu, K.; Cheng, P.; Wu, F.; Hong, B.; Yeager, K.M.; et al. Late Holocene Indian summer monsoon variations recorded at Lake Erhai, Southwestern China. *Quat. Res.* **2015**, *83*, 307–314. [[CrossRef](#)]
81. Fleitmann, D.; Burns Stephen, J.; Mudelsee, M.; Neff, U.; Kramers, J.; Mangini, A.; Matter, A. Holocene Forcing of the Indian Monsoon Recorded in a Stalagmite from Southern Oman. *Science* **2003**, *300*, 1737–1739. [[CrossRef](#)]
82. Duan, K.; Yao, T.; Thompson, L.G. Low-frequency of southern Asian monsoon variability using a 295-year record from the Dasuopu ice core in the central Himalayas. *Geophys. Res. Lett.* **2004**, *31*, L16209. [[CrossRef](#)]
83. Chu, G.; Sun, Q.; Yang, K.; Li, A.; Yu, X.; Xu, T.; Yan, F.; Wang, H.; Liu, M.; Wang, X.; et al. Evidence for decreasing South Asian summer monsoon in the past 160 years from varved sediment in Lake Xinluhai, Tibetan Plateau. *J. Geophys. Res. Earth Surf.* **2011**, *116*, D02116. [[CrossRef](#)]
84. Xu, H.; Hong, Y.; Hong, B. Decreasing Indian summer monsoon intensity after 1860 AD in the global warming epoch. *Clim. Dyn.* **2012**, *39*, 2079–2088, Erratum in *Clim. Dyn.* **2012**, *39*, 2089. [[CrossRef](#)]
85. Mann, M.; Cane, M.; Zebiak, S.; Clement, A. Volcanic and Solar Forcing of the Tropical Pacific over the Past 1000 Years. *J. Clim.* **2005**, *18*, 447–456. [[CrossRef](#)]
86. Sun, Z.; Yuan, K.; Hou, X.; Ji, K.; Li, C.-G.; Wang, M.; Hou, J. Centennial-scale interplay between the Indian Summer Monsoon and the Westerlies revealed from Ngamring Co, southern Tibetan Plateau. *Holocene* **2020**, *30*, 1163–1173. [[CrossRef](#)]